High temperature optically stable spectrally-selective $Ti_{1-x}Al_xN$-based multilayer coating for concentrated solar thermal applications

M. Bilokur, A. Gentle, M. Arnold, M.B. Cortie* and G.B. Smith

School of Mathematical and Physical Sciences, University of Technology Sydney, Australia

*Corresponding author. *E-mail address*: michael.cortie@uts.edu.au

Abstract

Spectrally-selective solar absorbing coatings based on the $Ti_{1-x}Al_xN$ system were deposited using DC magnetron sputtering. Due to their refractory nature and very suitable optical properties, these were considered for high temperature solar thermal energy conversion. The composition of $Ti_{1-x}Al_xN$, (effectively, the Ti/Al ratio) was optimized to achieve a maximized solar absorptance. The optimum composition was then tested in a tandem absorber which included anti-reflective layers. A stainless steel substrate was used in order to simulate service in parabolic trough-based power plants that use stainless steel pipe to carry the heat-transfer fluid. High temperature annealing of the stack caused structural modifications but the solar absorptance of 92% was retained even after annealing at 900°C.

Keywords: spectrally selective coatings; solar absorbers; thermal stability; titanium aluminium nitride; solar thermal conversion; stacks

1. Introduction

In today's material science, nitrides have a special place due to their ability to achieve a wide spectrum of properties. Nitrides in combination with different elements of the periodic table may create structures with metallic, semiconductor or insulator-like behaviour. Metal nitride compounds are interesting as many of them have high chemical resistance, high thermal stability, wear resistance and are very hard. Such a broad variety of nitride phases with a wide range of structures and corresponding chemical and physical properties enables them to be successfully applied as optical and protective coatings,

ultraviolet radiation detectors, diffusion barriers, solar cells, heat mirrors and plasmonic materials.

A variety of metal-nitride tandems composed of Si_3N_4, AlN, TiAlON, WAlN, WSiAlN, TiCN, CrAlON, TiN and TiAlN thin layers have been designed to achieve high thermal stability and desired spectral selectivity for enhanced solar thermal conversion [1-9]. Among these, TiN is very widely used due to its structural simplicity (cubic NaCl), broad regions of homogeneity, efficient diffusion barrier properties, optical properties resembling gold, and a relatively easy deposition process (eg. arc vapour deposition or magnetron sputtering). However, to overcome rapid oxidation of the TiN at 500°C and to push the boundaries of thermal tolerance, additional elements such as Sc, Al, Cr, Nb have been introduced into the binary compound, with Al being a popular addition. Addition of the latter forms a cubic $Ti_{1-x}Al_xN$ phase with randomly distributed Ti and Al atoms within the metal sub-lattice [10-12]. This was successfully demonstrated in Munz's work [13], where $Ti_{0.5}Al_{0.5}N$ showed thermal tolerance up to 700°C in hot air, which was attributed to the formation of a protective aluminium oxide layer. Heat treatment at temperatures greater than 700°C led to a rapid oxidation of the $Ti_{0.5}Al_{0.5}N$ film. However, while extension of oxidation limits of the TiN was successfully achieved by introduction of Al, another problem, spinodal decomposition at ~800°C, set a new maximum operating temperature.

All $Ti_{1-x}Al_xN$ films produced to date show a tendency to decompose when heated. In Höglund's work, a thermally annealed $Ti_{0.51}Al_{0.49}N$ thin film at 1000°C in a vacuum ambient (5×10^{-4} Pa) showed oxidation and loss of Al into a vacuum chamber followed by spinodal decomposition into c-AlN and TiN-rich domains starting at 800°C with a clear phase separation at 1000°C [10]. A series of other studies also report a phase separation of the $Ti_{1-x}Al_xN$ into coherent c-AlN and c-TiN phases in the 800°C to 1000°C temperature range. The de-mixing of $Ti_{1-x}Al_xN$ into the more thermodynamically stable TiN and c-AlN is enabled by the higher rates of atomic diffusion that occur during annealing [14-16]. On the one hand, spinodal decomposition is known to have a positive effect in $Ti_{1-x}Al_xN$ systems for industrial applications, as a result of self-hardening of the cubic $Ti_{1-x}Al_xN$ but, on the other hand, any structural modification usually involves alteration in optical response of the material, which should be prevented in high temperature solar thermal applications. Introduction of a corrosive environment worsens the stability problem. For example, Cunha et al. showed decomposition of the $Ti_{1-x}Al_xN$ into AlN, Al_2O_3, TiO_2 and possible TiAlON in a very corrosive environment (H_2O-HCl)

during annealing at 350°C due to loss of nitrogen and consequential oxidation of metallic elements [17].

Despite the issue of possible decomposition, $Ti_{1-x}Al_xN$ is still a very suitable candidate as it has already been proven in practice to withstand high temperatures when used in efficient solar absorber coatings. Therefore, the goal of the current research was to explore the thermal stability and optical response of Al,Ti,N-based stacks that had been exposed to temperatures up to 900°C. In particular, we wished to discover whether possible decomposition of the TiAlN layers and other structural changes in the stack would affect its performance as a spectrally-selective coating (SSC).

A very high, solar absorptance α_s stable at temperatures in the range 600 to 1000°C is the central goal. It is calculated throughout this study using equation (1) with experimental data for the spectral reflectance R(λ) measured at ambient plus the ASTM AM 1.5D solar spectrum S(λ). R(λ,T) based on data from spectral ellipsometry taken at various temperatures up to 500°C was also used .

$$\alpha_S = \frac{\int_{0.3\ \mu m}^{2.5\ \mu m}(1-R(\lambda))S(\lambda)\mathrm{d}\lambda}{\int_{0.3\ \mu m}^{2.5\ \mu m}S(\lambda)\mathrm{d}\lambda} \quad (1)$$

2. Experimental details

The solar absorbing coating was deposited on a polished austenitic stainless steel (SS) substrate using a DC magnetron sputtering system. Prior to the deposition process, the vacuum chamber was evacuated to a base pressure of 2.8×10^{-6} Torr. The SS substrate was mechanically polished and then ultrasonically cleaned in an acetone and ethanol bath for 80 minutes in total. High purity targets Ti (99.99%), Al (99.9%), Pt (99.99%) and SiO_2 (99.99%) with a diameter of 50 mm were used for sputtering. The targets were cleaned for 1 minute in Ar-plasma prior to the deposition. A Pt IR back-reflector layer was deposited first, at an Ar pressure of 1.3 mTorr and an applied target current of 0.15 A. This was followed by an AlN diffusion barrier layer, which was deposited on a heated substrate with Ar and N_2 pressure being at 1.5×10^{-3} Torr and 2.4×10^{-3} Torr respectively. For the $Ti_{1-x}Al_xN$ layer, co-sputtering of the Ti and Al target was performed with

simultaneous introduction of N_2, with Ar and N_2 introduced into the chamber at 7×10^{-4} Torr and 1.1×10^{-3} Torr, respectively. Next, a second AlN layer, this time for anti-reflection (AR), was deposited. Finally, a RF power supply was used at 50 W for deposition of a top AR SiO_2 layer. The thickness of the thin films was controlled using a quartz crystal monitor installed inside the deposition chamber.

To test the potential of the SSCs for high temperature CSP applications, the multilayer stack was first exposed to high temperature annealing for 24 hours at 600°C in a vacuum tube furnace pumped down to 10^{-5} Torr and then to 24 hour annealing at 700°C, 750°C, 800°C, 2 hour annealing at 850°C and 3 hour annealing at 900°C, using a Denton thermal evaporation chamber pumped down to 10^{-5} Torr. The evolution of phases of the heat treated samples was observed *ex situ* using X-ray diffractometry employing a Bruker D8 Discover with LYNXEYE XE detector, Cu kα radiation (λ=1.54056 Å) operating at 40 kV and 40 mA and angle of incidence set at 8°.

The emittance of the coatings was measured using a custom-built emissometer heated to 82°C. A broadband thermopile sensor was used which detects thermal radiation over the 2.5 to 50 μm spectral range. The calibration of the instrument was performed using an Al reference sample. The spectral reflectance was obtained using an Agilent Cary 7000 Universal Measurement Spectrophotometer (UMS) covering wavelengths between 300 and 2500 nm. The angle of incidence was 8° off the surface normal.

Ellipsometry was conducted using a J.A. Woollam Co., Variable Angle Spectroscopic Ellipsometer (VASE). The ellipsometric parameters were measured between wavelengths of 300 to 3000 nm in 5 nm steps. Angles of 60, 70 and 75° were used. Following this, the refractive indices were extracted by fitting oscillator models using J.A. Woollams's WVASE software. The optical constants were used in turn to construct a theoretical model of the stack, once again using WVASE. The generated results were fitted to the experimentally measured ellipsometric parameters and measured reflectance spectra, with the thicknesses of the individual layers as variable parameters.

3. Design and structure

The theoretical design of the stack is shown in Fig. 1a. The Pt was chosen as the IR reflector due to high IR reflectance and thermal stability compared to other refractory metals tested such as Ta, W, V or Ni. Al or Ag also showed high values of the IR reflectance, but were not considered for this study due to their lower melting points.

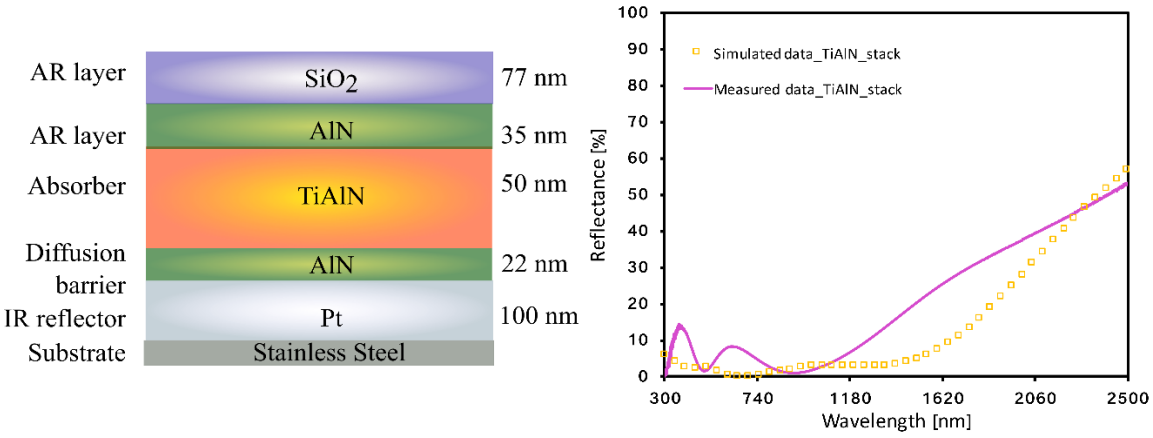

a) b)

Fig. 1. a) Design and b) comparison of the theoretical and measured optical response of the TiAlN-based stack using Pt as a back-reflector.

22 nm AlN was deposited on top of the Pt reflector in an attempt to retard upwards thermal diffusion from the Pt back-reflector or the SS substrate. The main absorbing layer was comprised of the $Ti_{1-x}Al_xN$ thin film, the Al/Ti ratio of which was carefully selected in order to achieve a maximum solar absorptance for the whole multilayer stack. Table 1 shows how the selected current applied to the Ti and Al targets affected the overall absorptance of the stack. Each $Ti_{1-x}Al_xN$ thin film was ellipsometrically measured and the determined optical constants were used to model the SSC and determine the theoretical solar absorptance. The layer with optimal deposition parameters resulted from an Al/Ti ratio that led to 95.6% solar absorptance of the SSC and was thus selected for the deposition within the stack. Two AR coatings, AlN and SiO_2, were deposited on top of the stack to reduce front reflection, along with the top AlN layer comprising an interference sandwich with the bottom AlN layer. The theoretical solar absorptance was

calculated based on the optical constants determined for each individual layer using ellipsometry. The resultant reflectance prediction is displayed in Fig.1b with a designed cut-off at 2000 nm. The theoretical model shows a broad, highly absorptive, region between 300 nm and 2000 nm. The experimental stack is a sandwich around the $Ti_{1-x}Al_xN$ and shows a more reflective response between 1200 nm and 2000 nm indicating a slightly more metallic nature in the main absorbing layer of the stack than in the single layer samples deposited in the initial optimization exercise. This may have been due to a higher vacuum (2.6×10^{-6} Torr) achieved in the deposition of the stack compared to 6.2×10^{-6} Torr obtained for the individual deposition of the $Ti_{1-x}Al_xN$ thin films. This factor leads to higher level of directionality of the sputtering metallic species and, as was shown in Table 1, may result in a reduction of solar absorptance by nearly 3% and higher reflectivity.

Table 1. The effect of Ti and Al target currents on the absorptance of the $Ti_xAl_{1-x}N$ based stack

Solar absorptance, %	**87.8**	**91.2**	**91.6**	**92.9**	**93.3**	**95.6**
Ti current, A	0.4	0.3	0.4	0.38	0.4	0.38
Al current, A	0.25	0.12	0.12	0.27	0.3	0.26

4. Optical characterization of the as-deposited solar absorber

The as-deposited solar absorber possesses a high level of spectral selectivity with minimized reflectance up to 2000 nm, Fig. 2, enabling achievement of a 92% solar absorptance. The 2000 nm cut-off was deliberately selected for the application of the absorber at 630ºC. This is due to the position of the black body spectrum, shifting towards shorter wavelengths when the sample is heated at higher temperatures, as shown in Fig. 3. Interference peaks also appear at around 350 nm and 600 nm due to the multilayer structure, but they have a relatively small negative effect on the solar absorptance. The SSC shows a steep reflectance ramp between 2000 nm and 4000 nm and nearly 100% reflectance in the thermal IR region, with measured thermal emittance, $\varepsilon_{82°C}$=0.04. The modelled emittance gave a slightly higher value of ε=0.11, which is attributed to the

optical constants of the layer up to 3000 nm predicting a minor reduction in the reflectance ramp.

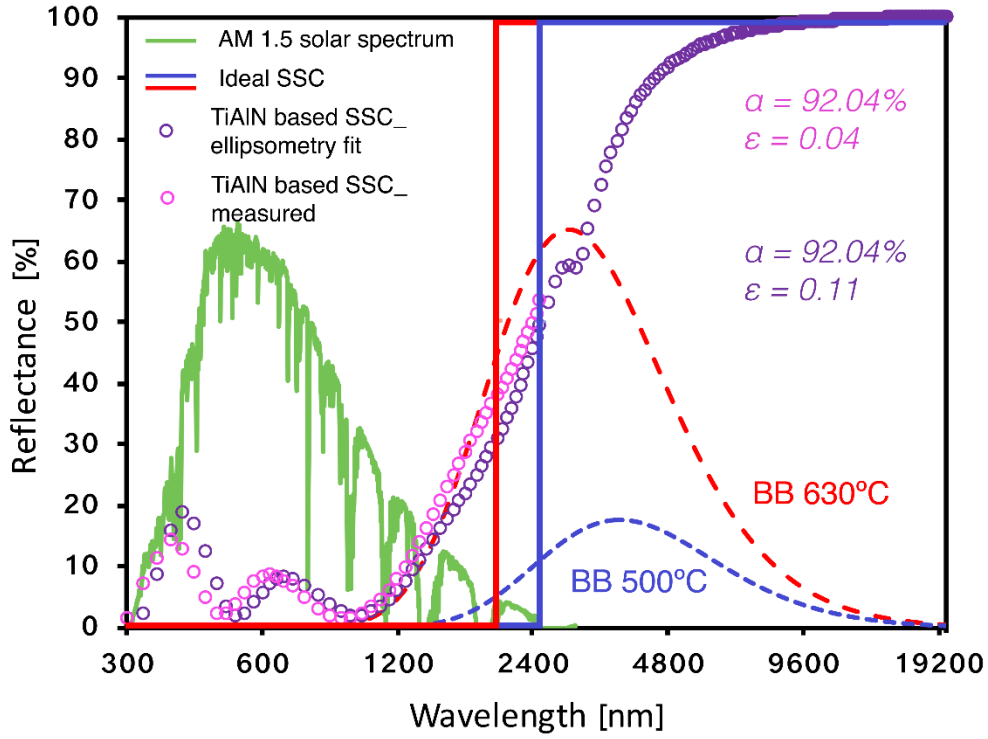

Fig. 2. Measured and modelled (ellipsometric fit to psi and delta of the stack) spectral selectivity of the SSC.

It is instructive to examine how high solar absorptance of the stack is built up as the succeeding layers are added. Fig. 3 shows the initial measured spectral response of an individual $Ti_xAl_{1-x}N$ layer on a Si substrate, followed by the addition of the other layers. The solar absorptance of the single $Ti_{1-x}Al_xN$ layer on Si was only 75%. Sandwiching this layer between two AlN films brought the solar absorptance up to 89%. Further enhancement in solar absorptance was achieved by the deposition of the top SiO_2 AR layer which contributed to a reduction in reflectance in the vis-near-IR, and an increase in solar absorptance to 92%.

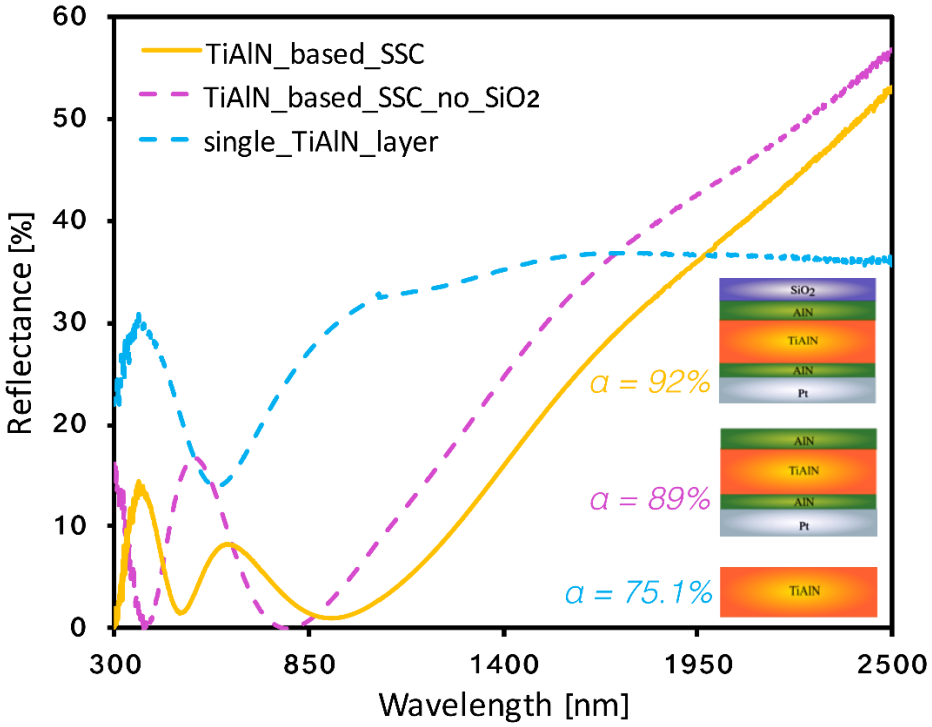

Fig. 3. Measured reflectance of the individual $Ti_xAl_{1-x}N$ layer on Si substrate, $Ti_xAl_{1-x}N$ on a SS substrate without the Ar SiO_2 layer, and the complete stack.

As demonstrated in Gunther's work, for single tracking parabolic trough power plants, the angular dependence of the spectrally selective solar absorber is important up to 32º incidence angle due to the geometry of the parabolic trough mirrors and their relative position to the absorbing pipe [18]. Fig. 4 demonstrates that the present coating has nearly unchanged solar absorptance to 30º incidence, with α staying above 90% up to 50º, after which absorptance declines monotonically to 60% at 80º incidence. This drop is predicted using the Fresnel interface equations.

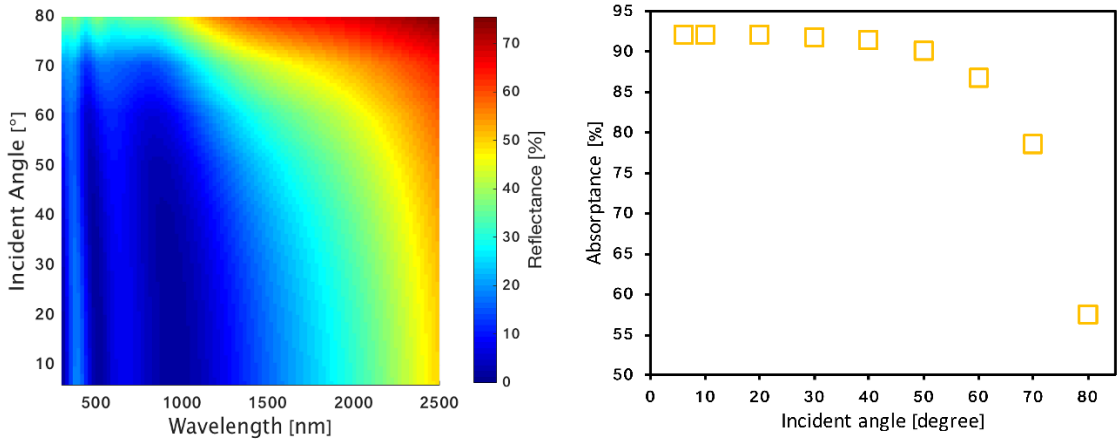

a) b)

Fig. 4. a) Modelled angular dependence of the reflectance and b) calculated angular dependent solar absorptance of the full $Ti_xAl_{1-x}N$ stack

5. Effect of temperature

Fig. 5 shows XRD diffraction patterns collected from the stack after each heat treatment. Unfortunately, the platinum back-reflector and, later, the SS substrate, dominate the patterns. No peaks for crystalline AlN or SiO_2 were detected, indicating an amorphous or poorly crystalline nature of these layers, as expected. XRD of the as-deposited stack shows that two face-centred cubic phases are present, one with a lattice parameter of about 3.93 Å and a strong 101 preferred orientation, and the other with a lattice parameter of about 4.15 Å . On the basis of its lattice parameter and its intensity (the high atomic number of Pt will cause it to dominate the XRD pattern), the former is likely to be the Pt layer, and the latter is $Ti_{1-x}Al_xN$ with $x \approx 0.5$. The existence of some Ti oxides cannot be excluded. These might be due to the presence of the residual oxygen in the vacuum chamber. The annealing of the stack at 600ºC results in the upward thermal diffusion of the Fe present in the SS substrate into the Pt IR reflecting layer, resulting in the formation of Fe_3Pt phase. The $Ti_{1-x}Al_xN$ is still present however, although its peaks are much smaller than those of Fe_3Pt. The effect this has on a spectral selectivity and the optical response of the stack will be discussed later. Further heat treatment at 800ºC and above causes the Pt in the Fe_3Pt to diffuse down into the substrate so that only the peaks for the austenite phase (F m -3 m, a=3.628 Å) of the substrate are visible. From this we conclude that the AlN diffusion barrier was not effective above 600 °C. In addition, an

AlN diffusion barrier should be deposited in future between the SS substrate and the Pt back reflector to avoid the formation of Fe_3Pt at the earlier stages of annealing,

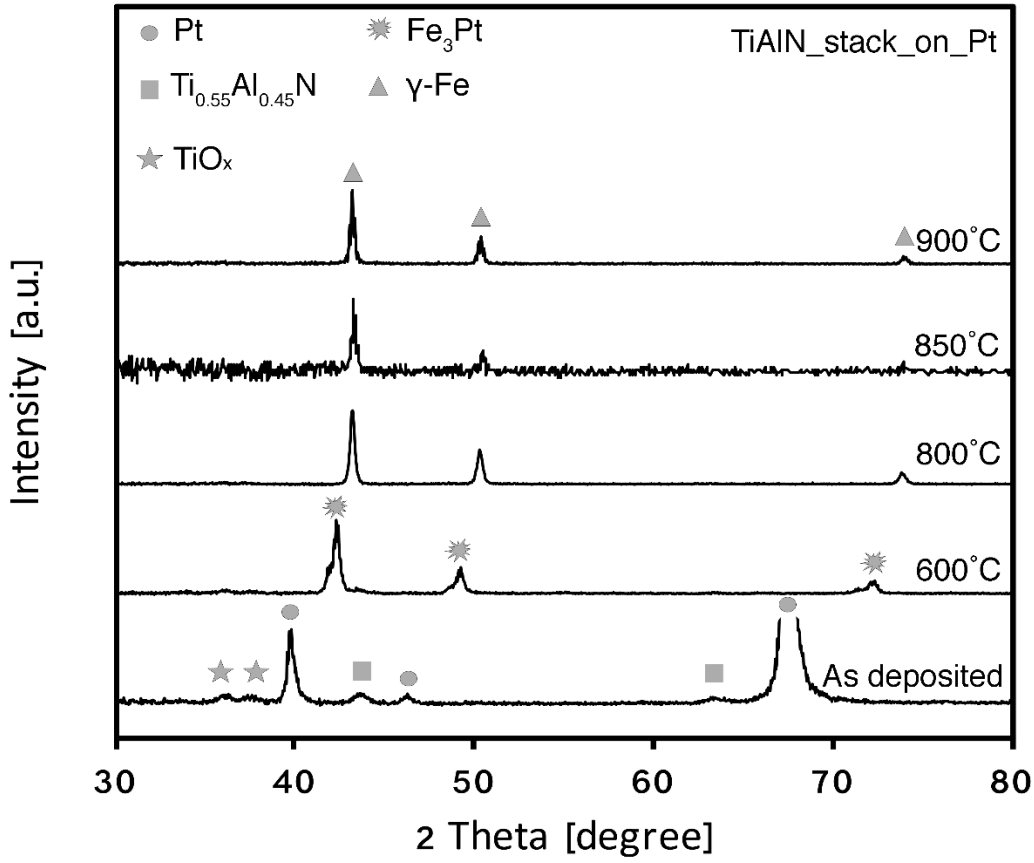

Fig. 5. The XRD patterns of the as-deposited and annealed stack.

Fig. 6 shows the ellipsometric fit to the measured psi parameters at different annealing temperatures up to 900ºC. These measurements were *ex situ* and were performed at room temperature. The high accuracy of the fits was achieved by fine adjustment of the oscillator parameters for the $Ti_{1-x}Al_xN$ absorbing layer and the thicknesses of the AR layers.

The stack undergoes noticeable changes in optical behaviour only after annealing at 800ºC and above. Up until that temperature the optical response is almost unchanged, as seen in the fixed position, widths and intensities of the psi peaks. The amplitude of the second peak in the psi parameter slightly increased after 600ºC and 700ºC anneals compared to the as-deposited conditions. The almost unchanged optical response shows that the Fe_3Pt layer is as good as the Pt one in terms of its performance as a back reflector.

However, after annealing for 24 hrs at 800ºC, a noticeable shift of the psi features occurs towards shorter wavelengths. The resulting optical behaviour is preserved upon further annealing at 900ºC. At this stage, it can be concluded that the dominant spectral behaviour of the stack is preserved up to 900ºC, at least for annealing times of the order of hours to tens of hours, even though the Fe of the substrate has diffused up through the stack.

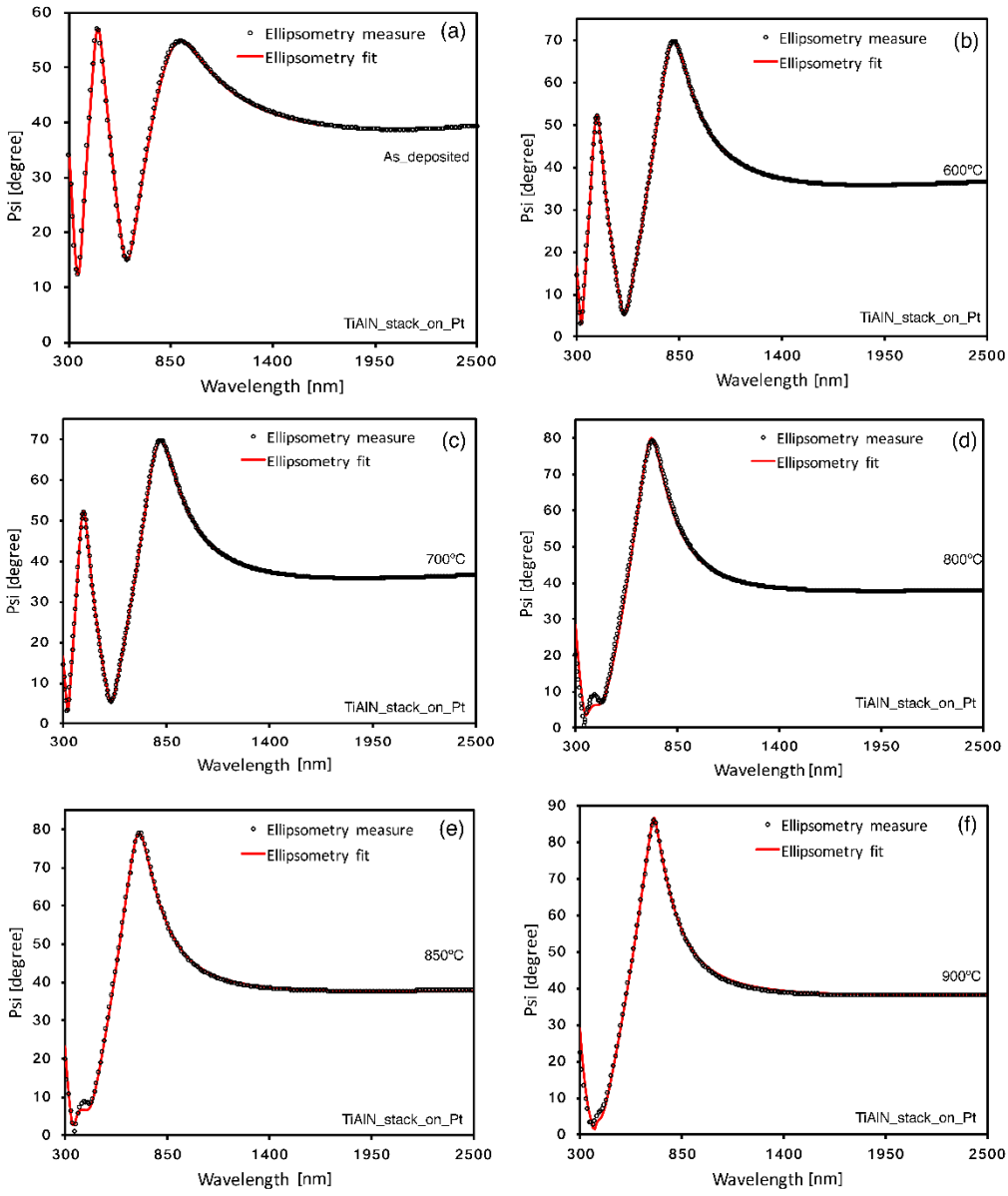

Fig. 6. Measured ellipsometric parameter psi and the fit after each stage of annealing in vacuum for 24 hrs (600 ºC -850ºC), 2hrs (850ºC) and 3 hrs (900ºC) of $Ti_{1-x}Al_xN$ based stack

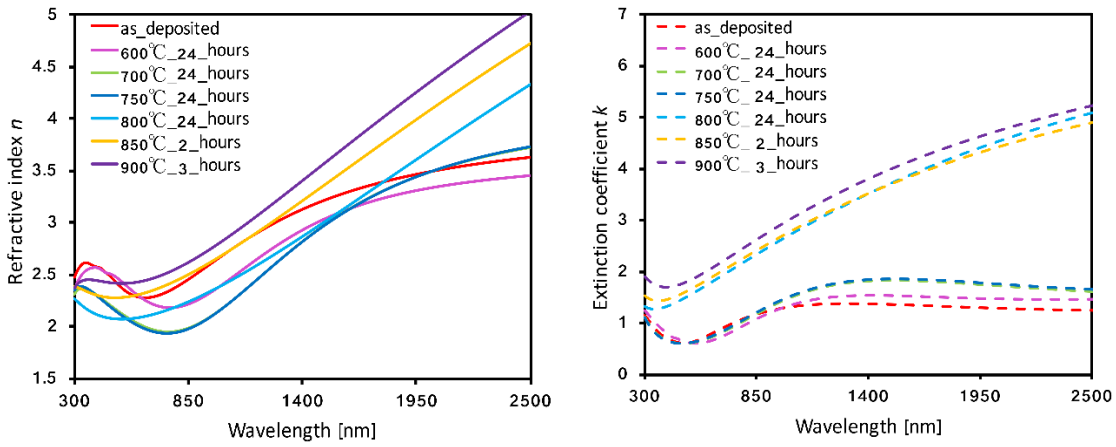

a) b)

Fig. 7. The evolution of the optical constants of the internal $Ti_xAl_{1-x}N$ layer a) *n* and b) *k* derived by fitting the measured ellipsometric parameters of each layer from Fig. 6 of the whole stack, which result after each stage of heat treatment.

The extracted *n, k* optical constants of the $Ti_{1-x}Al_xN$ absorbing layer are shown in Fig. 7. Up to 750°C, the coatings show semiconducting or semi-metal behaviour with $n > k$ throughout the whole wavelength range, but the refractive indices are relatively high due to the increasing metallic content.. The refractive indices *n* and *k* show a transitional behaviour between dielectric and metallic response. However, annealing above 750 °C has the effect of producing a metallic characteristic ($n < k$) for the longer wavelengths (>790 nm after annealing at 800°C, >600 nm after annealing at 800 and 900°C). In these cases the absorbing layer is optically denser with a stronger metallic behaviour as *k* increases over solar energy wavelengths. Comparison to published data for the refractive index of TiN suggests that, after annealing at 800°C and above, the $Ti_{1-x}Al_xN$ layer has lost some Al and has become more like TiN in its optical response.

The reflectance spectrum of the $Ti_{1-x}Al_xN$-based solar absorber shown in in Fig. 8 is very suitable for operating at 630ºC making the coating useful for use in photo-thermal conversion in current advanced parabolic trough solar power plants. The additional annealing up to 900ºC was conducted in order to test the potential of the stack for other high temperature solar thermal applications such as STPV. As demonstrated in Jurczak's work, the starting temperature for the exploitation of STPV using a SSC with a $Ga_xIn_{1-x}As$ semiconductor solar cell with bandgap of 0.4 eV would be 730ºC, for an efficiency of

15% [19]. For larger band-gaps higher operating temperatures are needed but higher efficiencies might also be achieved.

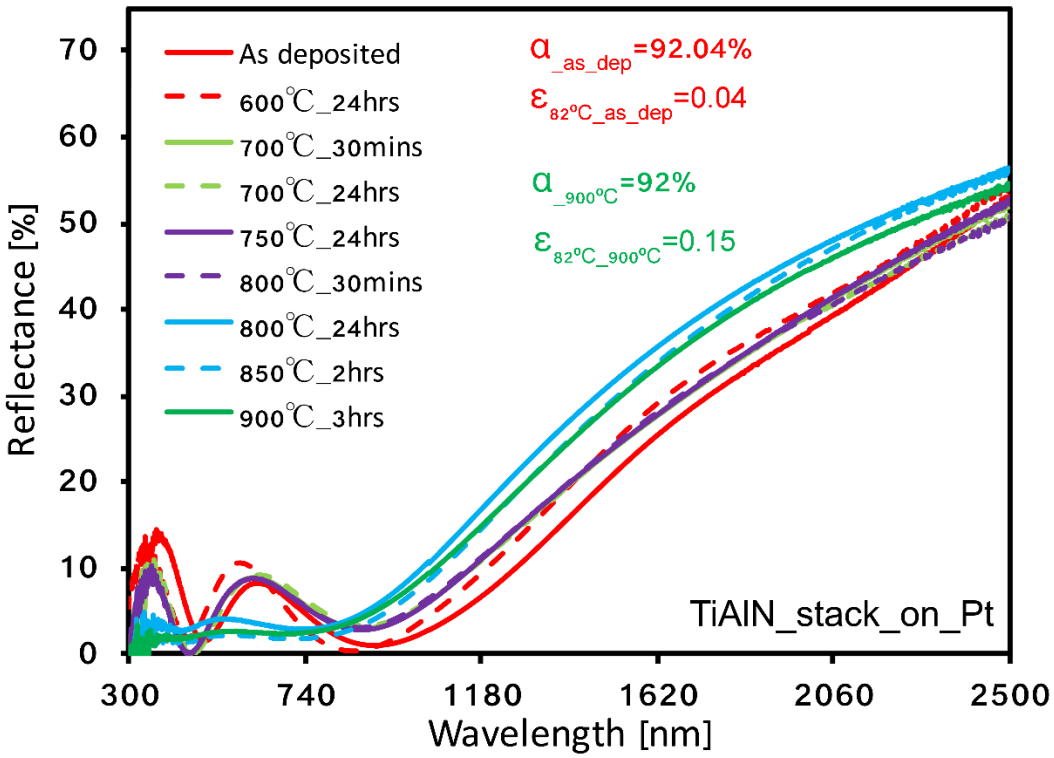

Fig. 8. The measured reflectance spectra of as-deposited and annealed $Ti_{1-x}Al_xN$ SSC up to 900 ºC in vacuum

The annealing of the $Ti_{1-x}Al_xN$-based stack up to 750ºC for 24 hours does not significantly affect the spectrally-selective response of the multilayer solar absorber. Fig. 9 shows that α_s varies only between the initial 92.0% to 91.2%. This is consistent with the ellipsometric measurements in Fig. 6, shown by the absence of significant changes in the ellipsometric parameters up to 700ºC annealing. Interestingly, further short-term annealing of the stack at 800ºC for 30 minutes does not affect the reflectivity of the sample compared to the preceding annealing stage at 750ºC, however, annealing of the sample at 800ºC for 24 hours leads to more noticeable changes in the spectral response. The disappearance of the two characteristic interference humps and flattening of the reflectance curve is beneficial in this case and results in enhanced absorptance in the region, 300 nm – 750 nm, where the highest intensity of solar radiation is located. On the other hand, there is a slight rise in the reflectance curve beyond 1000 nm. This behaviour could be attributed to two possible phenomena: either recrystallization of the metallic

back reflector, or structural modifications in the main absorbing layer. Both factors could be operating in the present case, with the increase in emittance from 0.04 to 0.15 after annealing at 900ºC due to the formation of some surface roughness and oxides, and destruction of the back-reflecting layer by dint of it reacting with the Fe of the substrate. (the latter was shown in the XRD patterns). Despite this, the α_s of the stack remained at 92% which compares well with the 96% of the original modelling which was based on models using *n* & *k* data of layers of individually deposited materials.

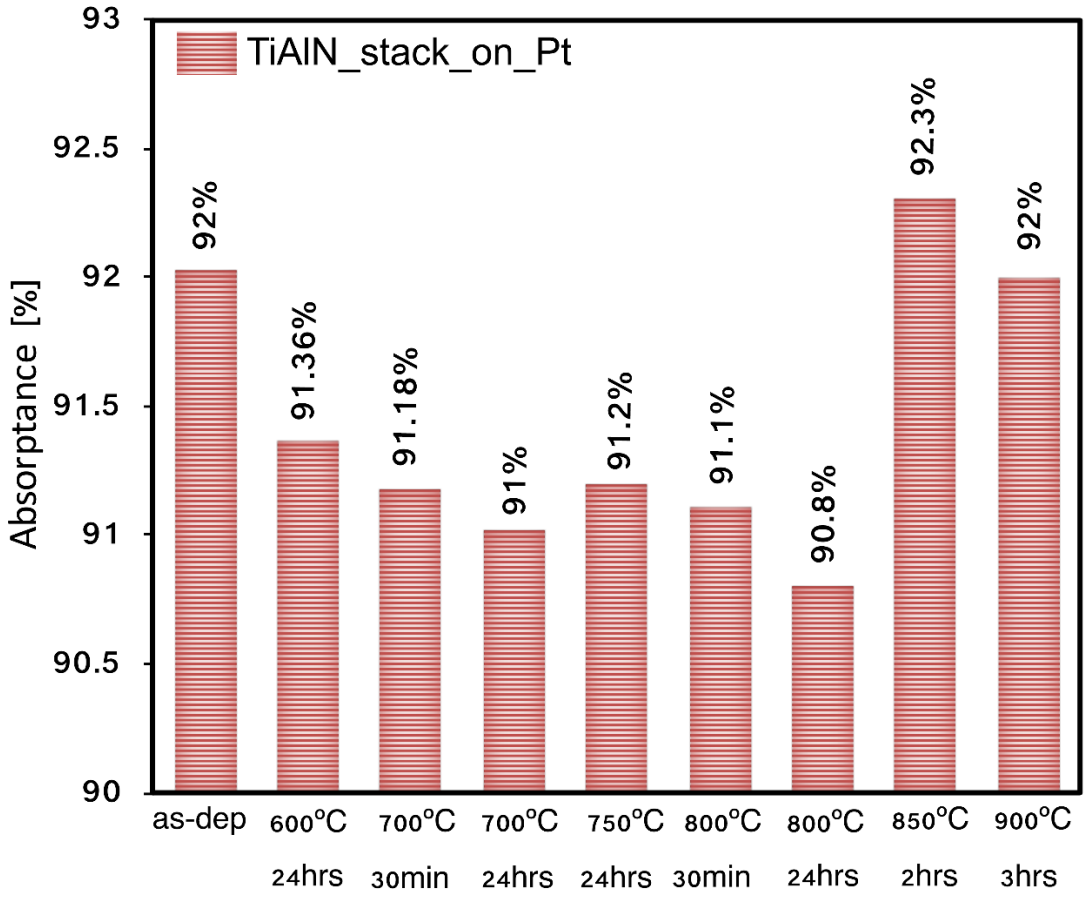

Fig. 9. Calculated α_s for as-deposited $Ti_xAl_{1-x}N$ and its post annealing value after 24 hours in vacuum at each temperature from a Pt IR reflector on the SS substrate.

From the preceding optical results, the efficiency η of solar photo-thermal conversion at 630ºC was calculated taking into account likely concentration factors C, and thermal emittance ε_s using

$$\eta = \frac{\alpha_S S_{total} - \varepsilon_S (T^4_{absorber} - T^4_{ambient})}{S_{total}} \quad (2)$$

with σ the Stefan – Boltzmann constant.

If one separates the right side of equation (2) into two parts, the weighting factor f_W for radiant loss over heat input of equation (3) is obtained.

$$f_w = \frac{\varepsilon_S (T^4_{absorber} - T^4_{ambient})}{S_{total}} \quad (3)$$

f_W thus defines the relative importance of concentration factor C, and radiant loss at operating temperature $T_{absorber}$. For $f_W < 1$, conversion efficiency is dominated by α_s, with the ε_s value contributing only a small drop in efficiency.

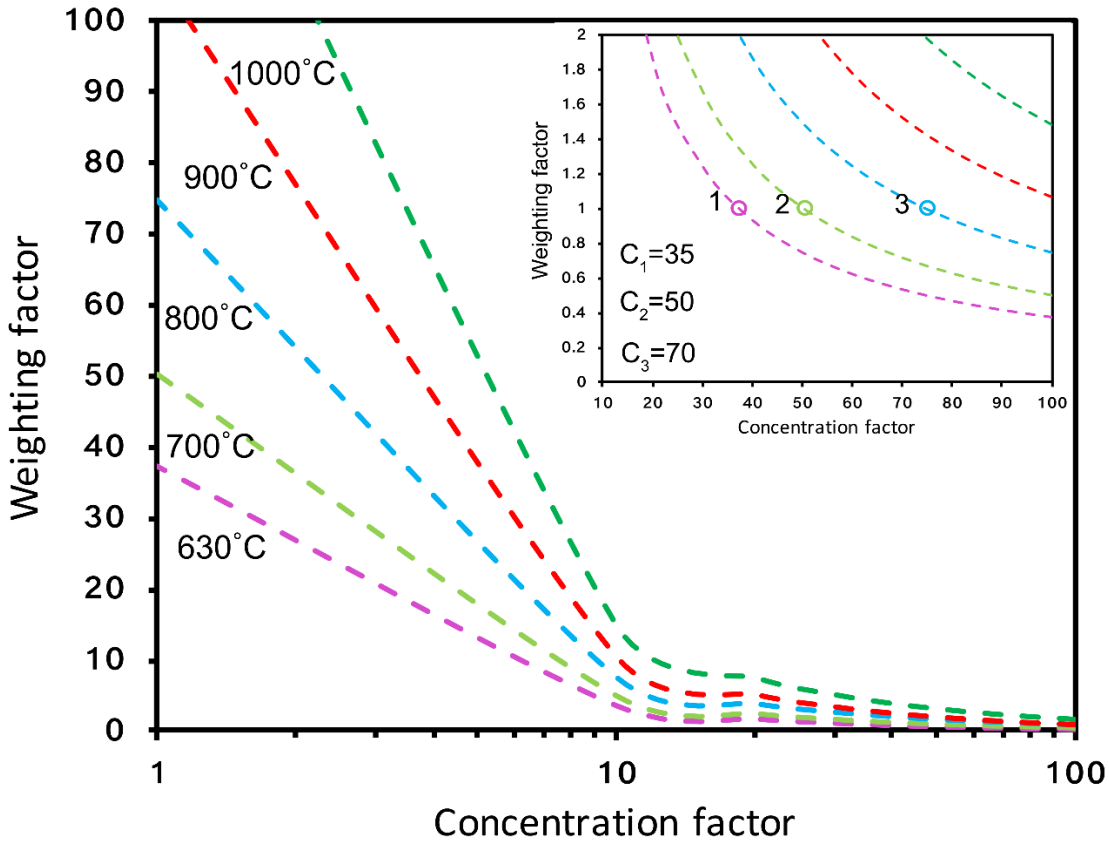

Fig. 10. The loss to input weighting factor as function of concentration factor at different operating temperatures for the optimum stack .The inset covers the *C* range where radiant loss has very small impact.

Fig. 10 shows this relation. With an increase in the absorber temperature, f_W rises, and a lower ε_s is then useful, but only an ε_s very close to zero in high vacuum could achieve *T* values around 600°C or above as plotted for *C* <10, so is not practical. On the other hand, an increase in the concentration factor raises efficiency with very little impact of ε_s and η continues to rise with a further rise in *C*. The inset in Fig. 10 shows where, on each plot, a rise in *C* value has a larger impact than the same relative reduction in ε_s. For operation at 630ºC, where this stack gives the maximum efficiency in a parabolic trough power plant, the solar flux S_1 should be concentrated by at least a factor of 35. A further increase in the concentration factor will raise T and reduce f_w. In this case α_s contributes even more to output efficiency η.

Fig. 11 demonstrates the influence of the concentration factor on the conversion efficiency for a range of solar absorbing surfaces all operating at 630ºC. The ideal SSC was set with $\alpha_s = 100\%$ and $\varepsilon_s = 0.01$. At these parameters, the ideal surface would convert 96% of solar radiation already if *C* = 1 sun and would reach 99.97% when *C* = 100. Our stack starts to achieve photo-thermal conversion at 630°C with just *C*=3.5, while the non-selective absorber needs at least *C*= 23. Thus high operating temperatures may also become possible with non-imaging collectors and an optimum $Ti_{1-x}Al_xN$ stack.

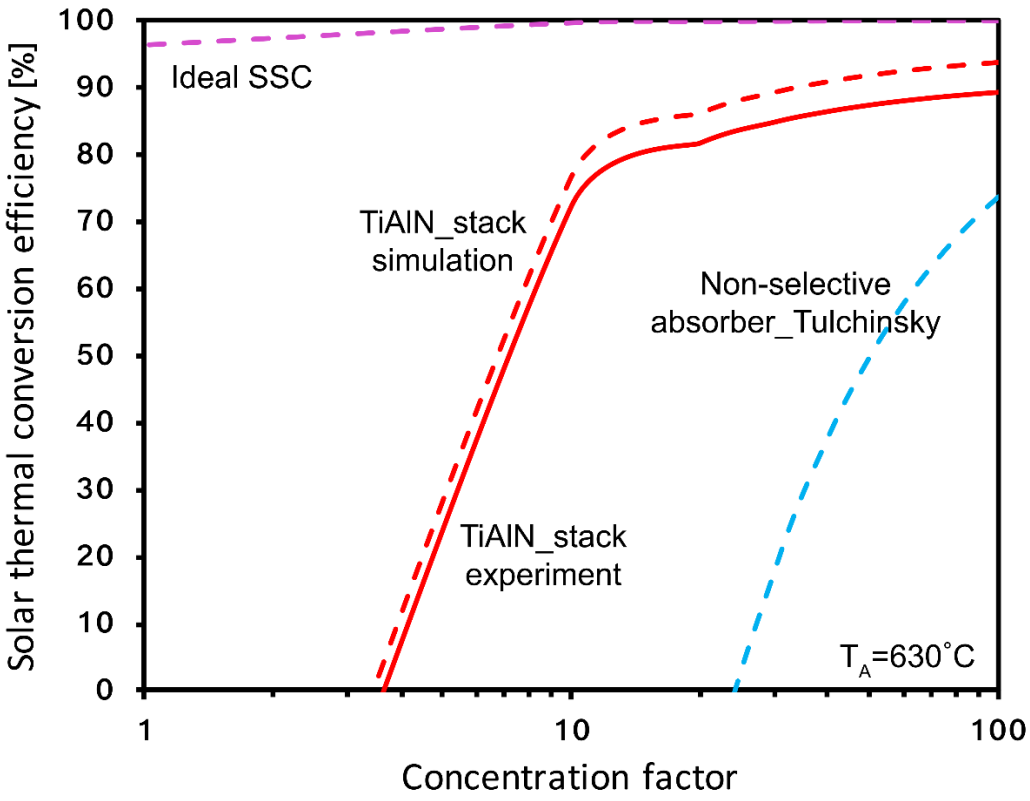

Fig. 11. The comparison of different absorbing surfaces contributing to the photo-thermal conversion efficiency as a function of concentration factor at operating temperature of 630ºC. The non-selective absorber described by Tulchinsky is included for comparison [20].

If both of them would be concentrated by a factor of 40, the modelled $Ti_{1-x}Al_xN$ SSC with expected solar absorptance of nearly 96% would convert solar radiation into useful heat with 92% efficiency and for the real deposited $Ti_xAl_{1-x}N$ SSC it would be converted at 82.2% efficiency. For C = 100 suns the possible designed heat conversion rate is 94% and 90% for the $Ti_{1-x}Al_xN$ stack reported herein after annealing to 600°C, for the modelled and real absorbing surfaces, respectively. The thermal emittance was taken as 0.051 for both modelled and deposited $Ti_{1-x}Al_xN$ stacks to highlight the influence of solar absorptance on efficiency. For C =100 or more, further improvement in solar absorptance as indicated from modelling would enable a boost in output by nearly 4%. The comparison demonstrated above, of the non-selective absorber obtained by Tulschinsky with α_s =97.4% and ε_{RT}=0.64, demonstrates that a lowering of emittance from 0.67 to 0.51. was very beneficial at 630°C. This non-selective surface would have a conversion

efficiency at 30 suns of 5% while our stack would yield 75%. At *C*=100 suns, the efficiency of the non-selective system would be 74%, which is ~17% lower than that obtained with our deposited $Ti_{1-x}Al_xN$ based selective stack.

6. Conclusions

A magnetron sputtered $Ti_xAl_{1-x}N$-based solar absorbing coating on an IR reflecting surface can achieve high optical stability and an excellent spectral selective response. A coating with nearly 96% solar absorptance was obtained by fine tuning the Ti/Al ratio. This material within a multi-layer stack consisting of a Pt back reflector coated with an AlN thin layer as a diffusion barrier layer, and with two antireflective layers AlN and SiO_2 on top. It displayed a high spectral selectivity ratio with its initial $\frac{\alpha_s}{\varepsilon_{82^oC}} = 0.92/0.04 = 23$. The experimental solar absorptance of 92%, compared well to the model of 96% based on our individual layer optical constants. Higher vacuum levels achieved during the extra time to sputter a stack was shown in ellipsometry to alter the previously obtained single layer optical constants beneficially. Reduced base pressure results in a greater directionality of the impacting sputtered ions on the substrate. Further tuning of deposition protocols to achieve 96% may still be possible. The stack containing $Ti_{1-x}Al_xN$ proved to be optically stable after each cycle of annealing in vacuum for 24 hours, at 600ºC, 700ºC, 750ºC, 800ºC, and for 2 hours at 850ºC and 3 hours at 900ºC. After annealing, spectral selectivity $\frac{\alpha_s}{\varepsilon_{82^oC}}$ dropped to 6.1 but solar absorptance barely changed, so at high *C* and *T*, a high output efficiency is maintained. $Ti_{1-x}Al_xN$ based solar absorbing stacks will thus be useful for long term operation in concentrated solar thermal applications at operating temperatures up to 800°C. They have potential with added refinement and testing for long term use up to 900ºC.

Acknowledgements

This work was supported by the Australian Research Council under grant DP140102003.

References

1. Du, M., X. Liu, L. Hao, X. Wang, J. Mi, L. Jiang, and Q. Yu, Microstructure and thermal stability of Al/$Ti_{0.5}Al_{0.5}N$/$Ti_{0.25}Al_{0.75}N$/AlN solar selective coating. *Solar Energy Mater. Solar Cells*, 2013. **111**: p. 49-56.
2. Feng, J., S. Zhang, Y. Lu, H. Yu, L. Kang, X. Wang, Z. Liu, H. Ding, Y. Tian, and J. Ouyang, The spectral selective absorbing characteristics and thermal stability of SS/TiAlN/TiAlSiN/Si_3N_4 tandem absorber prepared by magnetron sputtering. *Solar Energy*, 2015. **111**: p. 350-356.
3. Gao, X.-H., Z.-M. Guo, Q.-F. Geng, P.-J. Ma, A.-Q. Wang, and G. Liu, Enhanced optical properties of TiN-based spectrally selective solar absorbers deposited at a high substrate temperature. *Solar Energy Mater. Solar Cells*, 2017. **163**: p. 91-97.
4. Soum-Glaude, A., A. Le Gal, M. Bichotte, C. Escape, and L. Dubost, Optical characterization of $TiAlN_x$/$TiAlN_y$/Al_2O_3 tandem solar selective absorber coatings. *Solar Energy Mater. Solar Cells*, 2017. **170**: p. 254-262.
5. Liu, Y., C. Wang, and Y. Xue, The spectral properties and thermal stability of NbTiON solar selective absorbing coating. *Solar Energy Mater. Solar Cells*, 2012. **96**: p. 131-136.
6. Valleti, K., D.M. Krishna, and S. Joshi, Functional multi-layer nitride coatings for high temperature solar selective applications. *Solar Energy Mater. Solar Cells*, 2014. **121**: p. 14-21.
7. Barshilia, H.C., N. Selvakumar, K.S. Rajam, D.V.S. Rao, Muraleedharan, and A. Biswas, TiAlN/TiAlON/Si_3N_4 tandem absorber for high temperature solar selective applications. *Appl. Phys. Lett.*, 2006. **89**: p. 191909.
8. Dan, A., B. Basua, T. Echániz, I.G.d. Arrieta, G.A. López, and H.C. Barshilia, Effects of environmental and operational variability on the spectrally selective properties of W/WAlN/WAlON/Al_2O_3-based solar absorber coating. *Solar Energy Mater. Solar Cells*, 2018. **185**: p. 342–350.
9. Al-Rjoub, A., L. Rebouta, P. Costa, and L.G. Vieira, Multi-layer solar selective absorber coatings based on W/$WSiAlN_x$ /$WSiAlO_yNxSiAlO_x$ for high temperature applications. *Solar Energy Mater. Solar Cells*, 2018. **186**: p. 300-308.
10. Höglund, C., B. Alling, J. Birch, M. Beckers, P.O. Persson, C. Baehtz, Z. Czigány, J. Jensen, and L. Hultman, Effects of volume mismatch and electronic structure on the decomposition of ScAlN and TiAlN solid solutions. *Phys. Rev. B*, 2010. **81**(22): p. 224101.
11. Suh, C.-M., B.-W. Hwang, and R.-I. Murakami, Behaviors of residual stress and high-temperature fatigue life in ceramic coatings produced by PVD. *Mater. Sci. Eng. A*, 2003. **343**(1-2): p. 1-7.
12. Roos, J., J.-P. Celis, E. Vancoille, H. Veltrop, S. Boelens, F. Jungblut, J. Ebberink, and H. Homberg, Interrelationship between processing, coatingproperties and functional properties of steered arc physically vapour deposited (Ti, AI) N and (Ti, Nb) N coatings. *Thin Solid Films*, 1990. **193**: p. 547-556.
13. Münz, W.D., Titanium aluminum nitride films: A new alternative to TiN coatings. *J. Vacuum Sci. Technol. A: Vacuum, Surfaces, and Films*, 1986. **4**(6): p. 2717-2725.

14. Man, B., L. Guzman, A. Miotello, and M. Adami, Microstructure, oxidation and H_2-permeation resistance of TiAlN films deposited by DC magnetron sputtering technique. *Surface Coatings Technol.*, 2004. **180**: p. 9-14.
15. Abrikosov, I.A., A. Knutsson, B. Alling, F. Tasnádi, H. Lind, L. Hultman, and M. Odén, Phase stability and elasticity of TiAlN. *Materials*, 2011. **4**(9): p. 1599-1618.
16. Hörling, A., L. Hultman, M. Odén, J. Sjölén, and L. Karlsson, Thermal stability of arc evaporated high aluminum-content $Ti_{1-x}Al_x$ N thin films. *J. Vacuum Sci. Technol. A: Vacuum, Surfaces, and Films*, 2002. **20**(5): p. 1815-1823.
17. Cunha, L., M. Andritschky, L. Rebouta, and K. Pischow, Corrosion of CrN and TiAlN coatings in chloride-containing atmospheres. *Surface Coatings Technol.*, 1999. **116**: p. 1152-1160.
18. Gunther, M., M. Joemann, and S. Csambor, *Advanced CSP Teaching Materials, Chapter 5: Parabolic Trough Technology*. 2011, Enermena.
19. Jurczak, P., A. Onno, K. Sablon, and H. Liu, Efficiency of GaInAs thermophotovoltaic cells: the effects of incident radiation, light trapping and recombinations. *Optics Expresss*, 2015. **23**(19): p. A1208-A1219.
20. Tulchinsky, D., V. Uvarov, I. Popov, D. Mandler, and S. Magdassi, A novel non-selective coating material for solar thermal potential application formed by reaction between sol–gel titania and copper manganese spinel. *Solar Energy Mater. Solar Cells*, 2014. **120**: p. 23-29.